PCCP

PAPER

View Article Online
View Journal | View Issue

Cite this: *Phys. Chem. Chem. Phys.*, 2022, **24**, 3109

Understanding the evolution of the Raman spectra of molecularly p-doped poly(3-hexylthiophene-2,5-diyl): signatures of polarons and bipolarons†

Ahmed E. Mansour, ‡*[ab] Ana M. Valencia, ‡[ac] Dominique Lungwitz, [a] Berthold Wegner,[ab] Naoki Tanaka,§[d] Yoshiaki Shoji, [d] Takanori Fukushima, [d] Andreas Opitz, [a] Caterina Cocchi [ac] and Norbert Koch [ab]

Molecular doping is a key process to increase the density of charge carriers in organic semiconductors. Doping-induced charges in polymer semiconductors result in the formation of polarons and/or bipolarons due to the strong electron-vibron coupling in conjugated organic materials. Identifying the nature of charge carriers in doped polymers is essential to optimize the doping process for applications. In this work, we use Raman spectroscopy to investigate the formation of charge carriers in molecularly doped poly(3-hexylthiophene-2,5-diyl) (P3HT) for increasing dopant concentration, with the organic salt dimesityl borinium tetrakis(penta-fluorophenyl)borate (Mes_2B^+ $[B(C_6F_5)_4]^-$) and the Lewis acid tris(pentafluorophenyl)borane $[B(C_6F_5)_3]$. While the Raman signatures of neutral P3HT and singly charged P3HT segments (polarons) are known, the Raman spectra of doubly charged P3HT segments (bipolarons) are not yet sufficiently understood. Combining Raman spectroscopy measurements on doped P3HT thin films with first-principles calculations on oligomer models, we explain the evolution of the Raman spectra from neutral P3HT to increasingly doped P3HT featuring polarons and eventually bipolarons at high doping levels. We identify and explain the origin of the spectral features related to bipolarons by tracing the Raman signature of the symmetric collective vibrations along the polymer backbone, which – compared to neutral P3HT – redshifts for polarons and blueshifts for bipolarons. This is explained by a planarization of the singly charged P3HT segments with polarons and rather high order in thin films, while the doubly charged segments with bipolarons are located in comparably disordered regions of the P3HT film due to the high dopant concentration. Furthermore, we identify additional Raman peaks associated with vibrations in the quinoid doubly charged segments of the polymer. Our results offer the opportunity for readily identifying the nature of charge carriers in molecularly doped P3HT while taking advantage of the simplicity, versatility, and non-destructive nature of Raman spectroscopy.

Received 1st November 2021,
Accepted 9th January 2022

DOI: 10.1039/d1cp04985b

rsc.li/pccp

Introduction

The structural versatility of organic semiconductors, in addition to the feasible tunability of their electronic structure and electrical transport properties by doping have driven the development of low-cost, flexible, and efficient organic electronic and optoelectronic devices.[1–4] Molecular doping, defined as the process of adding a small amount of a molecule (dopant) to the organic semiconductor matrix (host), is key to increasing the density of free charge carriers as well as tuning the electronic structure of organic semiconductors.[5,6] Consequently, improved electrical conductivity and favorable interfacial energy level alignment can be achieved, towards high performance devices.[4,7–11] As a result of the strong coupling between charges and the local atomic structure (electron–vibron coupling) in organic semiconductors,

[a] *Institut für Physik & IRIS Adlershof, Humboldt-Universität zu Berlin, 12489 Berlin, Germany. E-mail: amansour@physik.hu-berlin.de*
[b] *Helmholtz-Zentrum Berlin für Materialien und Energie GmbH, 12489 Berlin, Germany*
[c] *Carl von Ossietzky Universität Oldenburg, Institute of Physics, 26129 Oldenburg, Germany*
[d] *Laboratory for Chemistry and Life Science, Institute of Innovative Research, Tokyo Institute of Technology, Yokohama 226-8503, Japan*

† Electronic supplementary information (ESI) available. See DOI: 10.1039/d1cp04985b

‡ These authors contributed equally to this work.

§ Present address: Department of Applied Chemistry, Graduate School of Engineering, Kyushu University, Fukuoka 819-0395, Japan.

doping-induced charges in polymers lead to a geometrical distortion of the polymer backbone, typically extending over a few monomer units.[12] Depending on the number of charges residing in such a geometrical distortion, the resulting species are classified as polarons and bipolarons. Polarons comprise one electron (hole) on the charged segment – equivalent to a radical anion (cation) of a molecule – and are characterized by the spin quantum number $S = \frac{1}{2}$. On the other hand, bipolarons comprise two electrons (holes) on the charged segment – equivalent to a dianion (dication) of a molecule – and are spinless carriers ($S = 0$).[12,13] The differentiation between polarons and bipolarons in doped polymers can be achieved using electron paramagnetic resonance spectroscopy (EPR), which directly probes charge carriers with $S = \frac{1}{2}$.[14–17] The aforementioned local relaxation of the polymer geometry of a polaron/bipolaron is coupled with a shift of, likewise localized, electronic energy levels into the energy gap of the polymer.[13,17–19] The energy of electronic transitions involving these intra-gap electronic states are characteristic of the type of the charge carriers, *i.e.* polarons or bipolarons. The electronic transitions can be probed using optical absorption spectroscopy, which is often used to identify the type of charge carriers in doped polymers and to quantify the density of polarons and bipolarons, as well as the ionization efficiency of the doping process.[8,15–17,20–22] Geometrical distortions on the charged polymer backbone have additionally offered means for probing polarons and bipolarons by investigating the associated changes in the charge-sensitive vibrational modes of doped polymers and oligomers using Raman spectroscopy and infrared absorption spectroscopy.[23–27]

Raman spectroscopy is a non-destructive and facile method that has proven to be highly suitable for studying polymer backbone structure and conformation.[28–31] This is a result of the strong electron-vibron coupling and the extended delocalization of the π-electrons in polymers, which lead to large cross-sections for Raman scattering and high sensitivity of the vibrational modes to structural changes.[28,32] The distinction of the charge-sensitive vibrational modes that are associated with polarons and bipolarons, if known, allows for a straightforward identification of the type of charge carriers and provides a tool to understand their correlation to molecular order and electrical properties.

Comprehensive understanding of the Raman spectra of poly(3-hexylthiophene-2,5-diyl) (P3HT) (shown in Fig. 1) and its related oligothiophene family has been established.[29,30,33,34] The characteristic peaks of vibrational modes involving the carbon atoms in the thiophene ring (C_α: atoms adjacent to the sulfur atom, and C_β: atoms not bonded to the sulfur atom) appear at frequencies in the range of 1300 cm^{-1} to 1600 cm^{-1}. The vibrational mode involving the C_β–C_β bond is typically observed at ~1350 cm^{-1}. C_α–C_β related vibrational modes are collective modes, in which several adjacent thiophene rings vibrate either in-phase or out-of-phase, and are strongly Raman active.[35] These modes include: (1) the symmetric vibration $[C_\alpha–C_\beta]_{sym}$ at ~1450 cm^{-1}, and (2) the asymmetric vibration $[C_\alpha–C_\beta]_{asym}$ at ~1500 cm^{-1}. Dispersion of the Raman peaks was observed with the length of oligomers (corresponding to the effective conjugation length in polymers).[28,33] In the case of oligothiophenes, when increasing the length of the oligomer, the modes $[C_\alpha–C_\beta]_{sym}$ and $[C_\alpha–C_\beta]_{asym}$ shift to lower energies, and, in addition, $[C_\alpha–C_\beta]_{asym}$ decreases in intensity. In P3HT, the $[C_\alpha–C_\beta]_{asym}$ mode is often only detectable as a tiny shoulder next to the more intense $[C_\alpha–C_\beta]_{sym}$.[33]

Polaron formation in electrochemically and molecularly doped P3HT has been associated with a redshift of the $[C_\alpha–C_\beta]_{sym}$ peak,[23,24] similar to the shifts observed once a radical cation is formed in doped pentathiophene (5T)[26] and doped sexithiophene (6T).[27] Nightingale *et al.* have identified the vibrational modes associated with polarons in P3HT by performing a comprehensive analysis of the Raman spectra in electrochemically doped P3HT.[23] The peak associated to the $[C_\alpha–C_\beta]_{sym}$ mode was deconvoluted into four contributing species: (1) ordered neutral chains, (2) disordered neutral chains, (3) ordered charged chains with polarons, and (4) disordered charged chains with polarons. Changes in the Raman spectrum associated with bipolaron formation were reported for $FeCl_3$ vapor-doped P3HT, which were characterized by an apparent blueshift and broadening of the $[C_\alpha–C_\beta]_{sym}$ mode.[24] However, the vibrational modes associated with bipolarons were not distinctively identified. In addition, detailed understanding of the evolution of the Raman spectrum of pristine P3HT upon increasing molecular dopant concentration with initial polaron- and subsequent bipolaron-formation is not yet available.

Recently, it was demonstrated that the organic salt dimesityl borinium tetrakis(penta-fluorophenyl)borate (Mes_2B^+ $[B(C_6F_5)_4]^-$) (shown in Fig. 1) is a potent p-dopant for P3HT, capable of forming both polarons and bipolarons depending on dopant concentration.[15] The underlying doping mechanism was identified to proceed through an electron transfer to the Mes_2B^+, which then leaves the sample, while the $[B(C_6F_5)_4]^-$ acts as the counter-ion that stabilizes both polarons and bipolarons. With increasing dopant concentration, the majority charge carrier type was identified as polaron up to moderate dopant concentration, but beyond *ca.* 20% dopant concentration bipolarons were also formed as long as samples were kept in an inert environment.[15]

Herein, we investigate (Mes_2B^+ $[B(C_6F_5)_4]^-$) doped P3HT to identify the vibrational modes associated with bipolaron formation. We probe the evolution of the Raman spectrum of molecularly doped P3HT, as it transitions from a nominally neutral polymer to a p-doped polymer with mainly polarons, and finally to a highly doped polymer containing mainly bipolarons. We compare the evolution of the Raman spectrum of the aforementioned stages with the situation when doping of P3HT is performed with the Lewis acid tris(pentafluorophenyl) borane $[B(C_6F_5)_3]$ (see Fig. 1), which is known to support the formation of polarons only.[15,16,22,36,37] This seems to be related to the doping mechanism *via* proton transfer[36] and follow up equilibration.[38] In this analysis, Raman spectra for molecularly doped P3HT are measured as a function of dopant concentration, covering the range of both polaron and bipolaron formation. First-principles calculations based on density-functional theory are performed on model oligothiophenes with increasing length (*n*T, where *n* is the number of thiophene

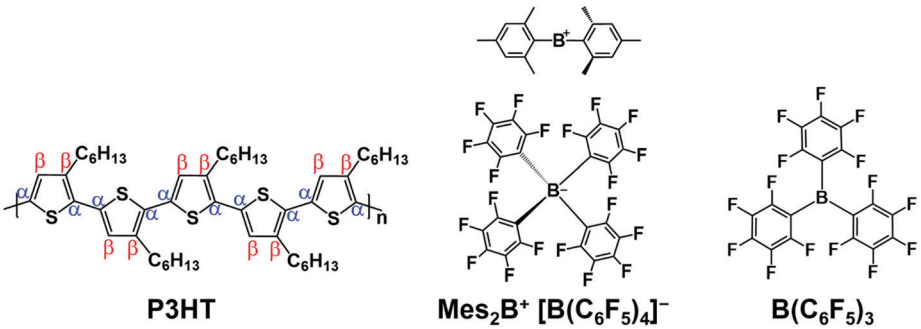

Fig. 1 Chemical structure of the materials employed in this work. The carbon atoms in P3HT are labeled according to their coordination: C_α are adjacent to a sulfur atom, while C_β are connected only to hydrogen and other carbon atoms.

units ranging from 2 to 6) to identify the vibrational normal modes in their radical cations and dications. Guided by the theoretical results, the experimental spectra are fitted to identify the vibrational modes associated with neutral chains, polarons, and bipolarons in P3HT, as well as their evolution as a function of dopant concentration. The changes of the Raman peak originating from the vibrational mode $[C_\alpha–C_\beta]_{sym}$ in P3HT chain segments containing either a polaron or a bipolaron are identified. Compared to the spectra of the neutral polymer, polarons result in a redshift of the Raman peak, while bipolarons result in a blueshift. These shifts are correlated to the effective conjugation lengths in the polymer within the framework of the effective conjugation coordinate model.[28] Our analysis reveals that charged P3HT chains with bipolarons exhibit a comparably short effective conjugation length due to the increased disorder in the film at high doping levels. This is in contrast to the case of charged P3HT chains with polarons, which appears to exhibit a larger effective conjugated length. Furthermore, we identify collective vibrational modes in charged P3HT associated with the concomitant quinoid structure (along the $C_\beta–C_\beta$ and inter-ring bonds), which significantly contribute to the broadening of main Raman peak $[C_\alpha–C_\beta]_{sym}$ in doped P3HT.

Results and discussion

Fig. 2 shows the changes in the Raman spectrum of P3HT thin film upon increasing dopant concentration with either $B(C_6F_5)_3$ (Fig. 2a) or Mes_2B^+ $[B(C_6F_5)_4]^-$ (Fig. 2b). The dopant concentration is defined as the percentage of the number of dopant molecules to the number of monomer units of P3HT in the mixed solution. The Raman spectrum of as-prepared P3HT comprises two characteristic peaks, corresponding to the $C_\beta–C_\beta$ vibration at $\sim$1374 cm^{-1} and to the $[C_\alpha–C_\beta]_{sym}$ vibration at $\sim$1439 cm^{-1}.

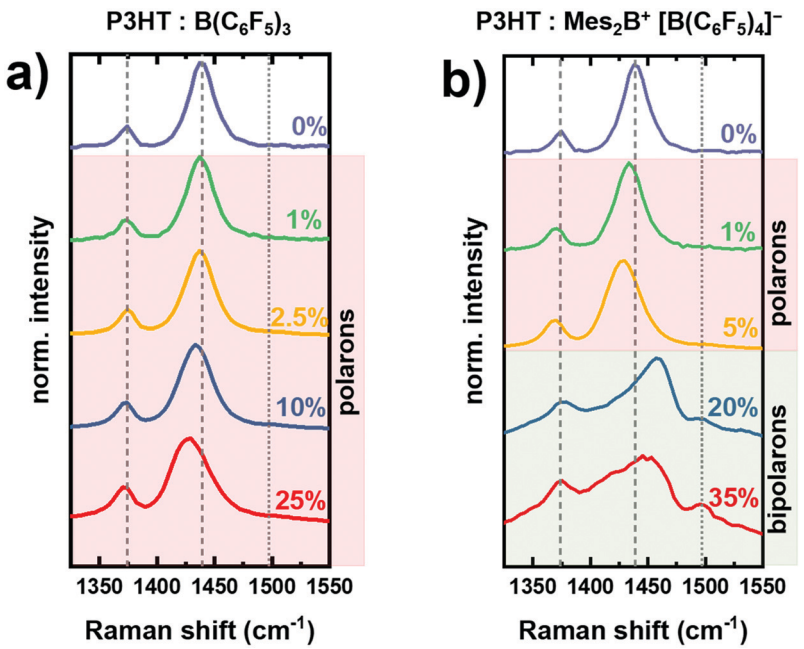

Fig. 2 Raman spectra of P3HT doped with (a) $B(C_6F_5)_3$ and (b) Mes_2B^+ $[B(C_6F_5)_4]^-$, as a function of the dopant concentration specified on each spectrum. The 0% indicates the as-prepared P3HT sample. Vertical dashed lines are introduced to guide the eyes in following the changes of the $[C_\alpha–C_\beta]_{sym}$ and $C_\beta–C_\beta$ vibrations, while the vertical dotted line is referred to the $[C_\alpha–C_\beta]_{asym}$ vibration.

We note that the presence of charged segments in the as-prepared P3HT film due to oxygen doping cannot be ruled out.[23,39]

First, we trace the changes of the Raman spectra of $B(C_6F_5)_3$-doped P3HT (Fig. 2a), in which polarons are the main charge carriers.[15,16,22,36] As the amount of $B(C_6F_5)_3$ increases, the peak associated with the $[C_\alpha–C_\beta]_{sym}$ mode progressively broadens and shifts towards lower energy, down to $\sim$1429 cm^{-1} at 25% dopant concentration. The broadening of the $[C_\alpha–C_\beta]_{sym}$ peak with increased dopant concentration results from the presence of differently ordered and charged P3HT chains in the film.[23] The redshift of the $[C_\alpha–C_\beta]_{sym}$ mode has been attributed to the increase of the bond length between $C_\alpha–C_\beta$ in doped P3HT, which subsequently leads to a reduction of the force constant of the collective vibration according to the effective conjugation coordinate model[23,28] and is characteristic to polaron formation, in agreement with previous reports on chemically doped P3HT with $FeCl_3$,[24,40] and electrochemically doped P3HT.[23,29] On the other hand, the peak associated with the $C_\beta–C_\beta$ vibration shows a negligible change, which agrees with previous reports on molecularly doped P3HT.[30] This can be attributed to the low charge-sensitivity of the $C_\beta–C_\beta$ vibration – as compared to the collective $C_\alpha–C_\beta$ vibration – to the changes in the (effective) conjugation length in (P3HT) oligothiophenes, which is the origin of the shifts in vibrational modes in charged polymers.

Next, we discuss the changes in the Raman spectra of Mes_2B^+ $[B(C_6F_5)_4]^-$ doped P3HT (Fig. 2b). Similar variations to the signals of the as-prepared samples as those described for $B(C_6F_5)_3$ doped P3HT are observed for low dopant concentrations of 1% and 5%. The $[C_\alpha–C_\beta]_{sym}$ vibration redshifts to $\sim$1429 cm^{-1} at 5% dopant concentration, indicating that the introduced charge carriers are mainly polarons at this doping level. As the dopant concentration increases further, the Raman spectrum drastically changes and broadens with an apparent blueshift of the $[C_\alpha–C_\beta]_{sym}$ vibration towards $\sim$1460 cm^{-1}. In addition, a peak assigned to the $[C_\alpha–C_\beta]_{asym}$ mode appears at 1500 cm^{-1}. It is not observed in the neutral P3HT and charged P3HT with mainly polaron, as shown by the vertical dotted line in Fig. 2.[33] Recently, we have conclusively confirmed the formation of bipolarons in Mes_2B^+ $[B(C_6F_5)_4]^-$ doped P3HT at dopant concentrations higher than 20% using EPR, optical absorption spectroscopy and photoemission spectroscopy.[15] Accordingly, we attribute the changes in the Raman spectra of Mes_2B^+ $[B(C_6F_5)_4]^-$ doped P3HT at dopant concentrations of 20% and 35% to bipolaron formation. Similar Raman signals compared to those shown in Fig. 2b (dopant concentration >20%) were also observed in $FeCl_3$ vapor doped P3HT, in which the blueshifted peak at 1470 cm^{-1} was considered as signature of bipolaron formation.[24] In addition, the observed broadening of the peak indicates the presence of differently structured and charged P3HT chains.

As a first step towards explaining the observed changes in the Raman spectra of doped P3HT, we compute the frequency of the $[C_\alpha–C_\beta]_{sym}$ and $[C_\alpha–C_\beta]_{asym}$ vibrational modes of the neutral oligothiophenes (2T, 3T, 4T, 5T and 6T) and identify the Raman active ones (see details in Table S1, ESI†). By increasing the oligomer length, the calculated vibrational frequencies for both $[C_\alpha–C_\beta]_{sym}$ and $[C_\alpha–C_\beta]_{asym}$ decrease (see Fig. S1, ESI†), in agreement with previous experimental and theoretical results.[28,30,33,41] We also checked that the Raman spectrum computed for the neutral 6T oligomer is in good agreement with previous results obtained from density-functional theory (b3lyp/6-31G*).[23,30] The redshift of the $C_\alpha–C_\beta$ modes from 2T to 6T is explained by the effective conjugation coordinate model: the force constant of the collective vibrations along the backbone of a conjugated oligomer/polymer decreases as the effective conjugation length increases.[23,28,35] This implies that the increasing oligomer length (or conformational order in polymer chains) results in lower energies for the vibrations along the backbone.

The calculated vibrational modes of the oligothiophene in the charged states exhibit clear differences as compared to the neutral case. For the considered oligothiophenes (2T, 4T and 6T) a distinct change in the structure is observed once the radical cations and dications are formed: the aromatic structure in the neutral state progressively turns into quinoid structure in the doubly-charged system, as shown in Fig. S2 (ESI†). We focus our subsequent discussion on the 6T oligomer since it more closely resembles the effective conjugation length in P3HT chains. Furthermore, considering the longer oligomer, there is a larger number of vibrational modes to be assigned. The assignment of the vibrational modes was based on the atomic displacements[35] and calculated Raman activity, which are detailed in the ESI,† see Table S2 and Fig. S5.

Focusing on the energy range of the experimental Raman fingerprints of P3HT, we compute the Raman spectra of 6T, $6T^{\bullet+}$ and $6T^{2+}$ shown in Fig. 3. The $[C_\alpha–C_\beta]_{sym}$ vibration of 6T gives rise to the intense peak at 1435 cm^{-1}, which redshifts to 1428 cm^{-1} in the spectrum of the radical cation, and blueshifts to 1440 cm^{-1} in the one of the dication. Furthermore, two additional Raman-active modes appear in the spectra of the charged 6T oligomers, namely, at 1408 cm^{-1} and at 1425 cm^{-1} for $6T^{\bullet+}$, and at 1409 cm^{-1} and 1429 cm^{-1} for $6T^{2+}$ (shown in Fig. S7, ESI†). Note that in Fig. 3, only the mode at $\sim$1409 cm^{-1} in both $6T^{\bullet+}$ and $6T^{2+}$ is included, while the higher energy peak is excluded since it obstructed the direct comparison of the changes in the $[C_\alpha–C_\beta]_{sym}$ vibrational mode. These results are in line with previously reported experimental data for 6T, in which the $[C_\alpha–C_\beta]_{sym}$ mode in the tetrafluoroborate-anion ($BF4^-$) doped 6T shifts to a lower energy of 1440 cm^{-1} as compared to the neutral 6T (1456 cm^{-1}) in the case of $6T^{\bullet+}$, with an obvious broadening towards the low energy in the range of 1400 cm^{-1} to 1430 cm^{-1}.[27] Once the dication is formed, the peak shifts towards higher energy at 1448 cm^{-1} with new peaks appearing at 1419 cm^{-1} and 1405 cm^{-1}.[27] The new Raman-active peaks appearing in the calculated and experimental spectra of the charged oligomers and of doped P3HT (in the range 1400 cm^{-1} to 1430 cm^{-1}) (Fig. S7, ESI†), seem to originate from stretching vibrations along the double bonds in quinoid structure (*i.e.*, along the $C_\beta–C_\beta$ and inter-ring bonds, see Fig. S6, ESI†).

Next, we turn to the measured Raman spectra of molecularly doped P3HT aiming to understand the spectral contributions of neutral and charged chain segments with either polarons or

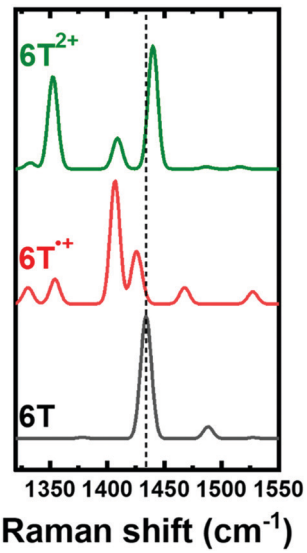

Fig. 3 Raman spectra calculated for sexithiophene oligomer in the neutral state (6T), in the radical cation ($6T^{\bullet+}$), and in the dication ($6T^{2+}$). A Gaussian broadening of 10 cm^{-1} is applied to all spectra. The quinoid structure related vibration at 1429 cm^{-1} was excluded in the simulation of the Raman spectra to clearly compare the shifts in the $[C_\alpha–C_\beta]_{sym}$ peak. See Fig. S7 (ESI†) for comparison of the quinoid structure related vibrations. The vertical dashed line traces the $[C_\alpha–C_\beta]_{sym}$ peak.

bipolarons. We consider the frequency range between 1350 cm^{-1}–1550 cm^{-1}, which includes both the $[C_\alpha–C_\beta]$ and $[C_\beta–C_\beta]$ vibration modes, and focus only on the $[C_\alpha–C_\beta]_{sym}$ vibrations. The experimental Raman spectrum (see Fig. 4) comprises several modes related to chains of different effective conjugation lengths and charged states. In the following peak fitting analysis, we consider neutral P3HT and P3HT chain segments containing polarons to be composed of two components for each charged state: (a) ordered chains, which exhibit longer effective conjugation lengths, and (b) disordered chains, characterized by shorter effective conjugation lengths. This assignment is justified by the fact the spin-coated regioregular P3HT results in semicrystalline films comprised of crystalline phases embedded in amorphous phases.[42]

Doping of both crystalline and amorphous phases have been reported in previous works.[16,22,23,43,44] In the case of polymer chains containing bipolarons, we consider a single peak to trace the $[C_\alpha–C_\beta]_{sym}$ vibrations, since bipolarons formation occurs at a high dopant concentration which typically results in increased amount of disordered regions in the film.[3,15]

The Raman spectra of as-prepared and charged P3HT with mainly polarons are fitted with four Gaussian peaks to model each of the charged states of P3HT (neutral and polarons) in either ordered or disordered chains, following the same procedure proposed by Nightingale *et al.*[23] and guided by our first-principles results (see Fig. 3). As shown in Fig. 4a, the peak associated to the $[C_\alpha–C_\beta]_{sym}$ vibration in as-prepared P3HT is deconvoluted to four main components: (1) neutral ordered chains, (2) neutral disordered chains, (3) charged ordered chain segments with polarons, and (4) charged disordered chain segments with polarons. The peak related to the neutral ordered chains appears at lower energy compared to the neutral disordered chains. This trend can be explained by the effective conjugation coordinate model, as mentioned earlier,[23] and it is further supported by our calculations, in which the $[C_\alpha–C_\beta]_{sym}$ vibration progressively shifts to lower energy as the oligomer lengths increases (see Fig. S1, ESI†). Additionally, the Raman peaks ascribed to P3HT chains containing polarons appears at lower energy in the as-prepared film: it is ascribed to oxygen doping, which is typically observed in as-prepared P3HT.[23,39] Upon doping with $B(C_6F_5)_3$, the peak due to the formation of polarons in disordered chains grows in intensity, which appears at a lower energy as compared to polarons in ordered chains as explained by Nightingale *et al.*[23] Inspecting the fittings shown in Fig. 4a, one can notice the progressively increasing intensity of the signatures of polaron-associated vibrations with increased dopant concentration at the cost of the decreasing intensity of the vibrations related to the

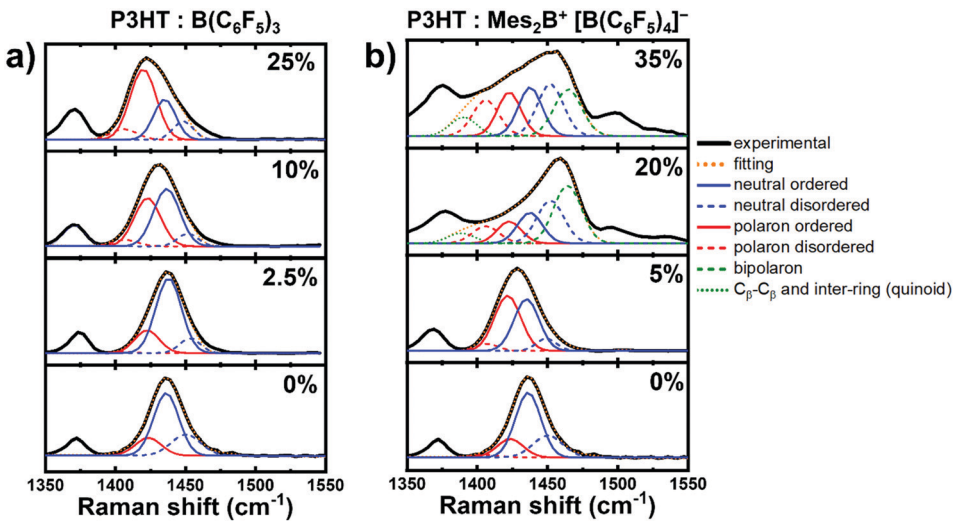

Fig. 4 Peak fitting analysis of the Raman spectra of doped P3HT with either (a) $B(C_6F_5)_3$ or (b) Mes_2B^+ $[B(C_6F_5)_4]^-$, with increasing dopant concentration.

neutral P3HT chains. Moreover, a shoulder can be observed at higher energy ($\sim$1465 cm^{-1}), which increases in intensity with the dopant concentration. This behavior can be ascribed to the $[C_\alpha–C_\beta]_{asym}$ vibrations, which are known to appear in the Raman spectra in oligothiophenes with an intensity and a frequency that are inversely proportional to the number of monomer units.[33] Accordingly, this shoulder is very small and close to the $[C_\alpha–C_\beta]_{sym}$ peak in the case of P3HT.[28,33] The increasing intensity of this shoulder with the dopant concentration indicates the increase of disorder, as evident by the relative growth of the peak intensities related to disordered chains in both neutral chains and polaron-containing chain segments. This implies the incrementing amount of polymer segments with shorter effective conjugation length, as the amount of dopant increases.

In the Raman spectra measured for Mes_2B^+ $[B(C_6F_5)_4]^-$ doped P3HT, similar fitting procedures (number of peaks and their positions and widths) are adopted for the dopant concentration of 5% where mostly polaron formation has been observed.[15] For the dopant concentrations of 20% and 35%, we extend the model by adding additional peaks to account for the formation of bipolarons (see Fig. 4b). The peak at $\sim$1466 cm^{-1} is due to the $[C_\alpha–C_\beta]_{sym}$ vibration of the chain segments containing bipolarons. The blueshift of the peak compared to that in the neutral case ($\sim$1438 cm^{-1}) agrees with the trend in the calculated Raman spectra of $6T^{2+}$ (Fig. 3). Furthermore, an additional peak is used to account for the broadening of Raman spectrum at around 1400 cm^{-1}, which is observed as a strong peak in the theoretical calculations of $6T^{2+}$. Our calculations demonstrate the existence of two strong symmetric vibrations along the $C_\beta–C_\beta$ and inter-ring bonds as shown in Fig. S6 (ESI†) (at 1409 cm^{-1} and 1429 cm^{-1}), which can be attributed to the formation of the quinoid structure in the doubly charged segments as discussed earlier (see Fig. S2, ESI†). We have excluded the quinoid structure related vibration at 1429 cm^{-1} in the peak fitting, as it coincides with the position of the vibration related to charged segments with polarons in disordered chains. The peak fitting analysis of the Mes_2B^+ $[B(C_6F_5)_4]^-$ doped P3HT at 20% and 35% dopant concentrations shows that the increase of the amount of the bipolarons is accompanied by a decrease of the amount of the polarons in the doped film as compared with doped films with mostly polarons (dopant concentration 5%). Implying that at higher dopant concentrations, charged segments with polarons become closer to each other, as well as, the ability of the Mes_2B^+ cation to remove electrons directly from a polaron favoring the formation of bipolarons.[15,45] Additionally, the amount of disorder in neutral chains and charged chain segments with polarons increases, as concluded from the increase in their respective fitted peaks (see Fig. 4). It is worth noting that the calculated vibrations indicate moderately active Raman modes at the frequency of the peak related to polarons in disordered chains (around 1424 cm^{-1}) that are due to asymmetrical vibrations along the $C_\beta–C_\beta$ and the inter-ring bonds in the quinoid structure in bipolarons. Thus, the peak ascribed to polarons in disordered chains can be interpreted a superposition of the new peaks, due to asymmetrical vibrations in the doubly charged quinoid segments, and the typically observed peak for polarons in disordered chains. Comparing the changes in the Raman spectrum between the dopant concentrations 20% and 35%, an apparent redshift around the $C_\alpha–C_\beta$ vibration can be observed. However, our peak fitting analysis suggests that the peak positions do not change, while the changing proportion of the peaks results in this apparent redshift. Increasing the dopant concentration from 20% to 35% results in an increase in the area of the peaks related polarons in both ordered and disordered segments. This indicates that further formation of polarons at higher dopant loadings is possible as well as the ability of the dopants to further dope disordered P3HT chains due to the strength of the dopant. However, we would like point out again that the peak related to the charged disordered segments with polarons coincides with the peak related to the quinoid structure vibrations at 1429 cm^{-1}, which seems to increase as inferred from the peak at 1409 cm^{-1}. A quantitative analysis of the type of charge carriers using our peak fitting analysis is not straightforward, and we stress that our analysis represents a qualitative description of the changes in the Raman spectra of P3HT with molecular doping.

Lastly, we explain the peaks appearing above 1500 cm^{-1}, which appear with large intensity only when bipolarons are present in the sample. These peaks are ascribed to $[C_\alpha–C_\beta]_{asym}$ vibrations in line with the calculated Raman spectra shown in Fig. 3 (see the assignments in Table S2 and Fig. S5, ESI†). The peak associated with the $[C_\alpha–C_\beta]_{asym}$ mode increases in intensity as the effective conjugation length decreases.[33] The large intensity of the peaks $\sim$1500 cm^{-1} in the case of bipolarons implies that charges are localized on shorter chain segments within the polymer.[28,33] The fact that such peaks are not visible in the spectrum of charged P3HT segments with polarons but are visible in the charged P3HT segments with bipolarons can be explained by the increased disorder in the latter system.

The presented results provide distinct signatures to differentiate P3HT neutral chains, chains with polarons, and chains with bipolarons using Raman spectroscopy. The strong peak associated to the $[C_\alpha–C_\beta]_{sym}$ mode in the spectrum of neutral chains redshifts in the case of charged chains with mainly polarons. This implies an increased effective conjugation length in charged P3HT with polarons accompanied by the planarization of the thiophene rings. Furthermore, doping of ordered regions of P3HT films is more energetically favorable as compared to doping of the disordered regions (see Fig. S8, ESI†).[16,23,46] This agrees with the progressive increase in the area of the peak related to polarons in ordered chain segments with increasing dopant concentration, while the peak related to polarons in disordered chain segments appears at higher dopant loadings (Fig. 4a), implying the possibility of doping the disordered domains in P3HT. In fact, Neelamraju *et al.* have demonstrated the possibility of integer charge transfer in F4TCNQ doped regiorandom P3HT.[46]

In the case of charged chains with bipolarons, the $[C_\alpha–C_\beta]_{sym}$ peak shifts to higher energy as compared to neutral and charged chains with polarons. This indicates that the effective conjugation length decreases in the charged polymer chains

with bipolarons. It is expected that bipolarons occur by further oxidation of the charged P3HT segments with polarons and thus converting them into charged segments with bipolarons. This is in general agreement with the changes in the EPR signal as the dopant concentration increases, which shows a decrease in the intensity of spin carrying carriers (polarons).[15] The observed blueshift of the vibration related to charged segments with bipolarons, and thus shorter effective conjugation length, is in contrast to the observed planarization in the calculated $6T^{2+}$ (see Fig. S4, ESI†). We explain this behavior by the larger amount of disorder in the film due to the increased presence of the counterions (which is not accounted for in the calculations),[47] as well as, the aggregation in the solution phase of mixed dopant–polymer solution. It has been demonstrated that heavily charged segments of the polymer chains lead to chain twisting and hence to significant bond length variations, as recently revealed in bipolaron charged P3HT oligomer model using time-dependent DFT and molecular dynamic simulations.[13] In previous work, we resolved different signatures in the optical absorption spectra of doped P3HT with polarons in ordered P3HT chains, and with polarons in isolated/disordered P3HT chains.[22] We notice that the high-energy polaron peak in the optical absorption spectra of ordered aggregates splits into two peaks at 1.3 eV and 1.65 eV, while in isolated charged chains it appears as a single peak at 1.5 eV. Using $B(C_6F_5)_3$ as dopant for P3HT, the transition from these split peaks in ordered and charged P3HT towards the single peak in isolated and disordered chains occurs at a dopant loading of 80%. On the other hand, the same transition occurs at 10% concentration in the case of the organic salt Mes_2B^+ $[B(C_6F_5)_4]^-$ is used as dopant, as demonstrated by Wegner *et al.*[15] This suggests that molecularly doped P3HT with Mes_2B^+ $[B(C_6F_5)_4]^-$ is more prone to disorder and thus results in shorter effective conjugation length than charged P3HT with mainly polarons.

Conclusion

In conclusion, we investigated the changes in the Raman spectrum of molecularly doped P3HT as it transitions from nominally neutral to doped with the presence of polarons only and to highly doped with bipolarons, as function of the dopant Mes_2B^+ $[B(C_6F_5)_4]^-$ concentration. The proposed analysis of the measured spectra agrees with calculated Raman spectra of the oligomers 6T, $6T^{\bullet+}$, and $6T^{2+}$. We demonstrated that the main Raman peak associated with the $[C_\alpha–C_\beta]_{sym}$ vibrations in neutral P3HT shifts to lower energy for P3HT with polarons, and to higher energy in presence of bipolarons. This implies that polaron formation results in a higher effective conjugation length and in good planarization of the charged chain segments, in contrast to bipolaron formation where a decrease of the effective conjugation length of charged chain segments occurs due to the increased amount of disorder. Furthermore, we identified two additional Raman active modes that are present for both polarons and bipolarons, originating from symmetrical and asymmetrical vibrations along the $C_\beta–C_\beta$ and inter-ring bonds in the quinoid structure of charged P3HT segments. Our results offer guidelines for investigating the presence of polarons and bipolarons in doped P3HT using Raman spectroscopy, and to understand the associated geometrical distortions. Even if the present results are for P3HT only, the discussion might stimulate the improved characterization of polarons and bipolarons in other polymers. Such knowledge combined with the versatility of Raman spectroscopy, for example *via in situ* measurements and nano-scale mapping, will aid in the future investigations and optimizations of molecular doping of polymers both in the solid state and in solution.

Experimental section

Materials and sample preparation

Two batches of P3HT were used in this study: (1) for doping with $Mes_2B^+[B(C_6F_5)_4]^-$, P3HT (weight average molecular weight M_w of 50–100 kg mol^{-1}, regioregularity >90%) from Sigma-Aldrich GmbH was used. (2) For doping studies with $B(C_6F_5)_3$, P3HT (M_w = 60.2 kg mol^{-1}, regioregularity of 97.6%) from Merck KGaA was used. $B(C_6F_5)_3$ was obtained from TCI Deutschland GmbH, while $Mes_2B^+[B(C_6F_5)_4]^-$) was synthesized as previously described.[48,49] Anhydrous chlorobenzene (CB) and 1,2-dichlorobenzene (*o*-DCB) were purchased from Sigma-Aldrich GmbH (>99.9% purity, inhibitor-free), and were further degassed *via* three freeze–pump–thaw cycles before using in solution preparation.

The doping technique used in this work is solution-mixed doping: (1) separate stock solutions of P3HT and the dopants were prepared inside a glovebox (<0.1 ppm H_2O, <0.1 ppm O_2), and stirred overnight. $Mes_2B^+[B(C_6F_5)_4]^-$ was dissolved in *o*-DCB, whereas CB was used as solvent for the doping with $B(C_6F_5)_3$. (2) The dopant solution and P3HT solution were mixed in a predefined volume proportions to control the dopant concentration.

Thin films were prepared *via* spin-coating using standard laboratory spin-coaters at various speeds (1000–6000 rpm) and times (1–2 min).

First-principles calculations

We performed first-principles calculations based on density functional perturbation theory (DFPT) to identify the vibrational modes in thiophene oligomers, commonly adopted as model systems for P3HT. A series of oligothiophenes (*n*T, where *n* is the number of thiophene units ranging from 2 to 6) is investigated to this end. For the calculation of Raman spectra, we do not consider the alkylation of the chains, since it has been demonstrated that alkyl chains do not substantially alter the electronic and optical properties of the thiophene backbones.[23,30,50] The optimized geometries and the vibrational modes of the neutral molecules are obtained in a spin-restricted formalism, while those of their radical cations ($nT^{\bullet+}$) associated to polarons, and their dications (nT^{2+}) associated to bipolarons are obtained in a unrestricted framework. We calculate both equilibrium geometries and vibrational force fields of all oligomers in the

ground and charged (+1 and +2) states.[23,34] In all calculations, the Perdew–Burke–Ernzerhof (PBE) exchange correlation functional[51] is adopted, in light of good results delivered by this approximation for organic crystals,[52] whereby also anharmonic effects were considered, and for hybrid organic/inorganic interfaces.[53] *Light* basis sets as implemented in FHI-aims package are adopted.[54,55] We checked that with these parameters lead to differences up to 4 cm^{-1} in the vibrational frequencies of the C–C modes. The calculated frequencies are reported without any scaling factor.

Raman spectroscopy

Raman spectra were obtained using an XploRA Plus Raman microscope (Horiba, Inc), using a 638 nm laser excitation, focused with a 100× objective. The laser intensity was attenuated to 1% of the initial laser intensity using optical filters, to prevent damage to the samples during measurements. The scattered signal was dispersed using 600 mm^{-1} grating, and was finally collected with cooled (−70 °C) Andor CCD detector.

P3HT doped with $Mes_2B^+[B(C_6F_5)_4]^-$ samples were measured without exposure to air, using a special encapsulation setup, with a Mica window to allow for Raman measurements.

Conflicts of interest

The authors declare no conflict of interest.

Acknowledgements

This work was funded in part by the Deutsche Forschungsgemeinschaft (DFG) – Projektnummer 182087777 – SFB 951. A. M. V. and C. C. acknowledge additional financial support from the German Federal Ministry of Education and Research (Professorinnenprogramm III) as well as from the State of Lower Saxony (Professorinnen für Niedersachsen).

References

1 H. Bronstein, C. B. Nielsen, B. C. Schroeder and I. McCulloch, the role of chemical design in the performance of organic semiconductors, *Nat. Rev. Chem.*, 2020, **4**, 66–77, DOI: 10.1038/s41570-019-0152-9.

2 A. C. Arias, J. D. MacKenzie, I. McCulloch, J. Rivnay and A. Salleo, Materials and applications for large area electronics: Solution-based approaches, *Chem. Rev.*, 2010, **110**(1), 3–24, DOI: 10.1021/cr900150b.

3 I. E. Jacobs and A. J. Moulé, Controlling molecular doping in organic semiconductors, *Adv. Mater.*, 2017, **29**(42), 1–39, DOI: 10.1002/adma.201703063.

4 N. Koch, Organic electronic devices and their functional interfaces, *Chem. Phys. Chem.*, 2007, **8**(10), 1438–1455, DOI: 10.1002/cphc.200700177.

5 I. Salzmann, G. Heimel, M. Oehzelt, S. Winkler and N. Koch, Molecular electrical doping of organic semiconductors: Fundamental mechanisms and emerging dopant design rules, *Acc. Chem. Res.*, 2016, **49**(3), 370–378, DOI: 10.1021/acs.accounts.5b00438.

6 B. Lüssem, M. Riede and K. Leo, Doping of organic semiconductors, *Phys. Status Solidi*, 2013, **210**(1), 9–43, DOI: 10.1002/pssa.201228310.

7 P. Pingel and D. Neher, Comprehensive picture of P-type doping of P3HT with the molecular acceptor F4TCNQ, *Phys. Rev. B*, 2013, **87**(11), 115209, DOI: 10.1103/physrevb.87.115209.

8 V. Untilova, J. Hynynen, A. I. Hofmann, D. Scheunemann, Y. Zhang, S. Barlow, M. Kemerink, S. R. Marder, L. Biniek, C. Müller and M. Brinkmann, High thermoelectric power factor of poly(3-hexylthiophene) through in-plane alignment and doping with a molybdenum dithiolene complex, *Macromolecules*, 2020, **53**(15), 6314–6321, DOI: 10.1021/acs.macromol.0c01223.

9 B. D. Naab, S. Himmelberger, Y. Diao, K. Vandewal, P. Wei, B. Lussem, A. Salleo and Z. Bao, High mobility N-type transistors based on solution-sheared doped 6,13-bis(triisopropylsilylethynyl)pentacene thin films, *Adv. Mater.*, 2013, **25**(33), 4663–4667, DOI: 10.1002/adma.201205098.

10 L. Ma, W. H. Lee, Y. D. Park, J. S. Kim, H. S. Lee and K. Cho, High performance polythiophene thin-film transistors doped with very small amounts of an electron acceptor, *Appl. Phys. Lett.*, 2008, **92**(6), 063310, DOI: 10.1063/1.2883927.

11 K. Walzer, B. Maennig, M. Pfeiffer and K. Leo, Highly efficient organic devices based on electrically doped transport layers, *Chem. Rev.*, 2007, **107**(4), 1233–1271, DOI: 10.1021/cr050156n.

12 J. L. Bredas and G. B. Street, Polarons, bipolarons, and solitons in conducting polymers, *Acc. Chem. Res.*, 1985, **18**(10), 309–315, DOI: 10.1021/ar00118a005.

13 I. Sahalianov, J. Hynynen, S. Barlow, S. R. Marder, C. Müller and I. Zozoulenko, UV-to-IR absorption of molecularly p-doped polythiophenes with alkyl and oligoether side chains: Experiment and interpretation based on density functional theory, *J. Phys. Chem. B*, 2020, **124**(49), 11280–11293, DOI: 10.1021/acs.jpcb.0c08757.

14 J. C. Scott, P. Pfluger, M. T. Krounbi and G. B. Street, Electron-spin-resonance studies of pyrrole polymers: Evidence for bipolarons, *Phys. Rev. B*, 1983, **28**(4), 2140–2145, DOI: 10.1103/PhysRevB.28.2140.

15 B. Wegner, D. Lungwitz, A. E. Mansour, C. E. Tait, N. Tanaka, T. Zhai, S. Duhm, M. Forster, J. Behrends, Y. Shoji, A. Opitz, U. Scherf, E. J. W. List-Kratochvil, T. Fukushima and N. Koch, An Organic borate salt with superior P-doping capability for organic semiconductors, *Adv. Sci.*, 2020, 2001322, DOI: 10.1002/advs.202001322.

16 M. Arvind, C. E. Tait, M. Guerrini, J. Krumland, A. M. Valencia, C. Cocchi, A. E. Mansour, N. Koch, S. Barlow, S. R. Marder, J. Behrends and D. Neher, Quantitative analysis of doping-induced polarons and charge-transfer complexes of poly(3-hexylthiophene) in solution, *J. Phys. Chem. B*, 2020, **124**(35), 7694–7708, DOI: 10.1021/acs.jpcb.0c03517.

17 C. Enengl, S. Enengl, S. Pluczyk, M. Havlicek, M. Lapkowski, H. Neugebauer and E. Ehrenfreund, Doping-induced absorption bands in P3HT: Polarons and bipolarons, *ChemPhysChem*, 2016, **17**(23), 3836–3844, DOI: 10.1002/cphc.201600961.

18 G. Heimel, The optical signature of charges in conjugated polymers, *ACS Cent. Sci.*, 2016, **2**(5), 309–315, DOI: 10.1021/acscentsci.6b00073.

19 S. Winkler, P. Amsalem, J. Frisch, M. Oehzelt, G. Heimel and N. Koch, Probing the energy levels in hole-doped molecular semiconductors, *Mater. Horiz.*, 2015, **2**(4), 427–433, DOI: 10.1039/C5MH00023H.

20 C. Wang, D. T. Duong, K. Vandewal, J. Rivnay and A. Salleo, Optical measurement of doping efficiency in poly(3-hexylthiophene) solutions and thin films, *Phys. Rev. B*, 2015, **91**(8), 085205, DOI: 10.1103/PhysRevB.91.085205.

21 A. I. Hofmann, R. Kroon, S. Zokaei, E. Järsvall, C. Malacrida, S. Ludwigs, T. Biskup and C. Müller, Chemical doping of conjugated polymers with the strong oxidant magic blue, *Adv. Electron. Mater.*, 2020, **6**(8), 2000249, DOI: 10.1002/aelm.202000249.

22 A. E. Mansour, D. Lungwitz, T. Schultz, M. Arvind, A. M. Valencia, C. Cocchi, A. Opitz, D. Neher and N. Koch, The optical signatures of molecular-doping induced polarons in poly(3-hexylthiophene-2,5-diyl): Individual polymer chains *versus* aggregates, *J. Mater. Chem. C*, 2020, **8**(8), 2870–2879, DOI: 10.1039/C9TC06509A.

23 J. Nightingale, J. Wade, D. Moia, J. Nelson and J. Kim, impact of molecular order on polaron formation in conjugated polymers, *J. Phys. Chem. C*, 2018, **122**(51), 29129–29140, DOI: 10.1021/acs.jpcc.8b09706.

24 J. Yamamoto and Y. Furukawa, Electronic and vibrational spectra of positive polarons and bipolarons in regioregular poly(3-hexylthiophene) doped with ferric chloride, *J. Phys. Chem. B*, 2015, **119**(13), 4788–4794, DOI: 10.1021/jp512654b.

25 A. Sakamoto, Y. Furukawa and M. Tasumi, Resonance Raman characterization of polarons and bipolarons in sodium-doped poly(*p*-phenylenevinylene), *J. Phys. Chem.*, 1992, **96**(9), 3870–3874, DOI: 10.1021/j100188a055.

26 Y. Furukawa, N. Yokonuma, M. Tasumi, M. Kuroda and J. Nakayama, Raman studies of doped polythiophene and the radical cation and dication of quinquethiophene, *Mol. Cryst. Liq. Cryst. Sci. Technol. Sect. A: Mol. Cryst. Liq. Cryst.*, 1994, **256**(1), 113–120, DOI: 10.1080/10587259408039238.

27 N. Yokonuma, Y. Furukawa, M. Tasumi, M. Kuroda and J. Nakayama, Electronic absorption and Raman studies of BF_4^--doped polythiophene based on the spectra of the radical cation and dication of α-sexithiophene, *Chem. Phys. Lett.*, 1996, **255**(4–6), 431–436, DOI: 10.1016/0009-2614(96)00383-1.

28 C. Castiglioni, M. Del Zoppo and G. Zerbi, Vibrational Raman spectroscopy of polyconjugated organic oligomers and polymers, *J. Raman Spectrosc.*, 1993, **24**(8), 485–494, DOI: 10.1002/jrs.1250240804.

29 G. Louarn, M. Trznadel, J. P. Buisson, J. Laska, A. Pron, M. Lapkowski and S. Lefrant, Raman spectroscopic studies of regioregular poly(3-alkylthiophenes), *J. Phys. Chem.*, 1996, **100**(30), 12532–12539, DOI: 10.1021/jp960104p.

30 W. C. Tsoi, D. T. James, J. J. S. J.-S. S. Kim, P. G. Nicholson, C. E. Murphy, D. D. C. C. Bradley, J. Nelson and J. J. S. J.-S. S. Kim, The nature of in-plane skeleton Raman modes of P3HT and their correlation to the degree of molecular order in P3HT:PCBM blend thin films, *J. Am. Chem. Soc.*, 2011, **133**(25), 9834–9843, DOI: 10.1021/ja2013104.

31 B. Sainbileg, Y.-B. Lan, J.-K. Wang and M. Hayashi, Deciphering anomalous Raman features of regioregular poly(3-hexylthiophene) in ordered aggregation form, *J. Phys. Chem. C*, 2018, **122**(8), 4224–4231, DOI: 10.1021/acs.jpcc.8b00326.

32 S. Wood, J. R. Hollis and J.-S. Kim, Raman spectroscopy as an advanced structural nanoprobe for conjugated molecular semiconductors, *J. Phys. D: Appl. Phys.*, 2017, **50**(7), 073001, DOI: 10.1088/1361-6463/50/7/073001.

33 Y. Furukawa, M. Akimoto and I. Harada, Vibrational key bands and electrical conductivity of polythiophene, *Synth. Met.*, 1987, **18**(1–3), 151–156, DOI: 10.1016/0379-6779(87)90870-8.

34 J. Yin, Z. Wang, D. Fazzi, Z. Shen and C. Soci, First-principles study of the nuclear dynamics of doped conjugated polymers, *J. Phys. Chem. C*, 2016, **120**(3), 1994–2001, DOI: 10.1021/acs.jpcc.5b11764.

35 L. Brambilla, C. Capel Ferrón, M. Tommasini, K. Hong, J. T. López Navarrete, V. Hernández and G. Zerbi, Infrared and multi-wavelength Raman spectroscopy of regio-regular P3HT and its deutero derivatives, *J. Raman Spectrosc.*, 2018, **49**(3), 569–580, DOI: 10.1002/jrs.5301.

36 B. Yurash, D. X. Cao, V. V. Brus, D. Leifert, M. Wang, A. Dixon, M. Seifrid, A. E. Mansour, D. Lungwitz, T. Liu, P. J. Santiago, K. R. Graham, N. Koch, G. C. Bazan and T.-Q. Nguyen, Towards understanding the doping mechanism of organic semiconductors by Lewis acids, *Nat. Mater.*, 2019, **18**, 1327–1334, DOI: 10.1038/s41563-019-0479-0.

37 C. E. Tait, A. Reckwitz, M. Arvind, D. Neher, R. Bittl and J. Behrends, Spin–spin interactions and spin delocalisation in a doped organic semiconductor probed by EPR spectroscopy, *Phys. Chem. Chem. Phys.*, 2021, **23**(25), 13827–13841, DOI: 10.1039/D1CP02133H.

38 C. C. Han and R. L. Elsenbaumer, Protonic acids: Generally applicable dopants for conducting polymers, *Synth. Met.*, 1989, **30**(1), 123–131, DOI: 10.1016/0379-6779(89)90648-6.

39 H.-H. Liao, C.-M. Yang, C.-C. Liu, S.-F. Horng, H.-F. Meng and J.-T. Shy, Dynamics and reversibility of oxygen doping and de-doping for conjugated polymer, *J. Appl. Phys.*, 2008, **103**(10), 104506, DOI: 10.1063/1.2917419.

40 L. C. T. Shoute, N. Pekas, Y. Wu and R. L. McCreery, Redox driven conductance changes for resistive memory, *Appl. Phys. A: Mater. Sci. Process.*, 2011, **102**(4), 841–850, DOI: 10.1007/s00339-011-6268-5.

41 H. E. Schaffer, R. R. Chance, R. J. Silbey, K. Knoll and R. R. Schrock, Conjugation length dependence of Raman scattering in a series of linear polyenes: Implications for polyacetylene, *J. Chem. Phys.*, 1991, **94**(6), 4161–4170, DOI: 10.1063/1.460649.

42 L. Brambilla, M. Tommasini, I. Botiz, K. Rahimi, J. O. Agumba, N. Stingelin and G. Zerbi, Regio-regular oligo and poly(3-hexyl thiophene): Precise structural markers from the vibrational spectra of oligomer single crystals, *Macromolecules*, 2014, **47**(19), 6730–6739, DOI: 10.1021/ma501614c.

43 P. Reiser, L. Müller, V. Sivanesan, R. Lovrincic, S. Barlow, S. R. Marder, A. Pucci, W. Jaegermann, E. Mankel and S. Beck, Dopant diffusion in sequentially doped poly(3-hexylthiophene) studied by infrared and photoelectron spectroscopy, *J. Phys. Chem. C*, 2018, **122**(26), 14518–14527, DOI: 10.1021/acs.jpcc.8b02657.

44 P. Y. Yee, D. T. Scholes, B. J. Schwartz and S. H. Tolbert, Dopant-induced ordering of amorphous regions in regiorandom P3HT, *J. Phys. Chem. Lett.*, 2019, **10**(17), 4929–4934, DOI: 10.1021/acs.jpclett.9b02070.

45 V. M. Geskin and J. L. Brédas, Polaron pair versus bipolaron on oligothiophene chains: A theoretical study of the singlet and triplet states, *Chem. Phys. Chem.*, 2003, **4**(5), 498–505, DOI: 10.1002/cphc.200200446.

46 B. Neelamraju, K. E. Watts, J. E. Pemberton and E. L. Ratcliff, Correlation of coexistent charge transfer states in F4TCNQ-doped P3HT with microstructure, *J. Phys. Chem. Lett.*, 2018, **9**(23), 6871–6877, DOI: 10.1021/acs.jpclett.8b03104.

47 S. N. Patel, A. M. Glaudell, K. A. Peterson, E. M. Thomas, K. A. O'Hara, E. Lim and M. L. Chabinyc, Morphology controls the thermoelectric power factor of a doped semiconducting polymer, *Sci. Adv.*, 2017, **3**(6), 24–26, DOI: 10.1126/sciadv.1700434.

48 Y. Shoji, N. Tanaka, K. Mikami, M. Uchiyama and T. Fukushima, A two-coordinate boron cation featuring C–B^{+}–C bonding, *Nat. Chem.*, 2014, (6), 498–503, DOI: 10.1038/nchem.1948.

49 Y. Shoji, N. Tanaka, D. Hashizume and T. Fukushima, The molecular and electronic structures of a thioaroyl cation formed by borinium ion-mediated C–S double bond cleavage of CS 2, *Chem. Commun.*, 2015, **51**(69), 13342–13345, DOI: 10.1039/C5CC05645D.

50 J. Krumland, A. M. Valencia and C. Cocchi, Exploring organic semiconductors in solution: the effects of solvation, alkylization, and doping, *Phys. Chem. Chem. Phys.*, 2021, **23**(8), 4841–4855, DOI: 10.1039/D0CP06085B.

51 J. P. Perdew, K. Burke and M. Ernzerhof, Generalized gradient approximation made simple, *Phys. Rev. Lett.*, 1996, **77**(18), 3865–3868, DOI: 10.1103/PhysRevLett.77.3865.

52 N. Raimbault, V. Athavale and M. Rossi, Anharmonic effects in the low-frequency vibrational modes of aspirin and paracetamol crystals, *Phys. Rev. Mater.*, 2019, **3**(5), 053605, DOI: 10.1103/PhysRevMaterials.3.053605.

53 L. Schöttner, S. Erker, R. Schlesinger, N. Koch, A. Nefedov, O. T. Hofmann and C. Wöll, Doping-induced electron transfer at organic/oxide interfaces: Direct evidence from infrared spectroscopy, *J. Phys. Chem. C*, 2020, **124**(8), 4511–4516, DOI: 10.1021/acs.jpcc.9b08768.

54 V. Blum, R. Gehrke, F. Hanke, P. Havu, V. Havu, X. Ren, K. Reuter and M. Scheffler, *Ab initio* molecular simulations with numeric atom-centered orbitals, *Comput. Phys. Commun.*, 2009, **180**(11), 2175–2196, DOI: 10.1016/j.cpc.2009.06.022.

55 H. Shang, N. Raimbault, P. Rinke, M. Scheffler, M. Rossi and C. Carbogno, All-electron, real-space perturbation theory for homogeneous electric fields: Theory, implementation, and application within DFT, *New J. Phys.*, 2018, **20**(7), 073040, DOI: 10.1088/1367-2630/aace6d.

